Chinese Journal of Aeronautics 25 (2012) 766-775

Contents lists available at ScienceDirect

Chinese Journal of Aeronautics

journal homepage: www.elsevier.com/locate/cja

# Nonlinear Adaptive Robust Force Control of Hydraulic Load Simulator

YAO Jianyong[a,b], JIAO Zongxia[a,*], YAO Bin[c], SHANG Yaoxing[a], DONG Wenbin[d]

[a] *Science and Technology on Aircraft Control Laboratory, Beihang University, Beijing 100191, China*

[b] *School of Mechanical Engineering, Nanjing University of Science and Technology, Nanjing 210094, China*

[c] *School of Mechanical Engineering, Purdue University, West Lafayette, IN 47907, USA*

[d] *Beijing Aerospace Automatic Control Institute, Beijing 100854, China*

Received 1 June 2011; revised 5 September 2011; accepted 26 September 2011

**Abstract**

This paper deals with the high performance force control of hydraulic load simulator. Many previous works for hydraulic force control are based on their linearization equations, but hydraulic inherent nonlinear properties and uncertainties make the conventional feedback proportional-integral-derivative control not yield to high-performance requirements. In this paper, a nonlinear system model is derived and linear parameterization is made for adaptive control. Then a discontinuous projection-based nonlinear adaptive robust force controller is developed for hydraulic load simulator. The proposed controller constructs an asymptotically stable adaptive controller and adaptation laws, which can compensate for the system nonlinearities and uncertain parameters. Meanwhile a well-designed robust controller is also developed to cope with the hydraulic system uncertain nonlinearities. The controller achieves a guaranteed transient performance and final tracking accuracy in the presence of both parametric uncertainties and uncertain nonlinearities; in the absence of uncertain nonlinearities, the scheme also achieves asymptotic tracking performance. Simulation and experiment comparative results are obtained to verify the high-performance nature of the proposed control strategy and the tracking accuracy is greatly improved.

*Keywords:* hydraulic load simulator; adaptive control; robust control; nonlinear control; hydraulic actuators; Lyapunov functions

## 1. Introduction

Electro-hydraulic load simulator (EHLS) [1-4] is a widely used hardware-in-loop-simulation assembly in flight control system development, which could simulate the air load executed in aircraft actuator system. Due to the direct connection between EHLS and the aircraft actuator, the operation of aircraft actuator leads to heavy disturbance to EHLS, which is also called extraneous force. Therefore EHLS is a typical electro-hydraulic force system strongly coupled with motion disturbance. How to eliminate the motion disturbance and improve EHLS tracking performance becomes the research hotspots in EHLS. To deal with the motion disturbance, the idea of the displacement/velocity synchronization is extensively used. In this area, Yu, et al. utilized an accessional hydraulic motor to keep the EHLS synchronization to the aircraft actuator so as to reduce the extraneous force [1]. Jiao, et al. investigated the disturbance source of EHLS and presented a velocity synchronous control method through importing the control input of aircraft actuator system [2]. A lot of forward compensation is also employed to eliminate the extraneous force [3-4]. Yao, et al. proposed an optimal scheme by online estimation of the system nonlinear gains and improved the tracking performance compared to the conventional PID contro-

*Corresponding author. Tel.: +86-10-82339238.
*E-mail address:* zxjiao@buaa.edu.cn
Foundation item: National Natural Science Foundation for Distinguished Young Scholars of China (50825502)


doi: 10.1016/S1000-9361(11) 60443-3

ller [5]. For low-speed-loading, LuGre model-based friction compensation is considered in Ref. [6].

To improve the robustness and tracking performance of EHLS, self-tuning proportional-integral-derivative (PID) control [7-8], quantitative feedback theory (QFT) method [9-13], inverse control [14], neural network [15-16] and compound feed-forward and feedback control [17] are investigated for EHLS control.

Many of the above-mentioned works are linear control methods. However, hydraulic systems also have a number of characteristics which complicate the development of high-performance closed-loop controllers. The dynamics of hydraulic systems are highly nonlinear [18]. Furthermore, the system may be subject to non-smooth and discontinuous nonlinearities due to control input saturation, directional change of valve opening, friction and valve overlap [19]. Aside from the nonlinear nature of hydraulic dynamics, hydraulic systems also have a large extent of model uncertainties, including uncertain parameters, such as the flow gain of servo valve, the coefficient of viscous damping, etc, and uncertain nonlinearities, such as un-modeled friction, external disturbance, etc. How to deal with these uncertainties is a challenge. Nonlinear inverse control [20] and adaptive and robust control [21] are employed for hydraulic nonlinear motion control.

In this paper, a nonlinear dynamic model of EHLS is derived, and uncertain parameters and nonlinearities are classified. A nonlinear adaptive robust controller is then constructed for hydraulic nonlinearities, unknown parameter and uncertain nonlinearities. A performance profile is discussed. To test the proposed controller, extensive simulation and experiment results are obtained.

## 2. Problem Formulation and Dynamic Models

The structure of electro-hydraulic load simulator and aircraft actuator system is shown in Fig. 1. The left is the unit under test (UUT), i.e. the aircraft actuator system, whose operation will produce motion disturbance to the right part, i.e. the electro-hydraulic load simulator. The goal of our controller design is to make the torque output to track any specified torque trajectory as closely as possible. In this controller design, the torque feedback, motion feedback (angle encoder) and pressure feedback (pressure sensor) are available.

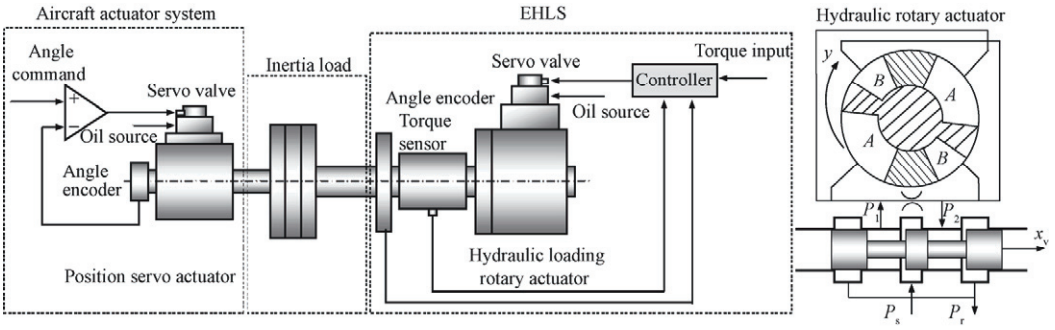


Fig. 1 Architecture of electro-hydraulic load simulator.

The dynamic of the EHLS torque output is

$$T = AP_{\mathrm{L}} - B\dot{y} - f(t, y, \dot{y}) \tag{1}$$

where $T$, $A$, $P_{\mathrm{L}}$, $B$, $y$ represent torque output, radian displacement of loading hydraulic rotary actuator, load pressure between the two chambers of the actuator, combined coefficient of the modeled damping and viscous friction forces, and the motion disturbance produced by aircraft actuator respectively; $f$ is the lumped uncertain nonlinearities due to external disturbances, the unmodeled friction forces and other hard-to-model terms; $P_{\mathrm{L}} = P_1 - P_2$, where $P_1$ and $P_2$ are the pressures inside the two chambers of the actuator. And in Fig. 1, $x_{\mathrm{v}}$ is the spool valve displacement of the servo-valve, $P_{\mathrm{s}}$ the supply pressure of the fluid, $P_{\mathrm{r}}$ the return pressure.

To improve the modeling accuracy, especially for the friction effect, we can use the following nonlinear approximation to represent the Coulomb friction:

$$\tilde{f}(t, y, \dot{y}) \triangleq f(t, y, \dot{y}) - A_{\mathrm{f}} S_{\mathrm{f}}(\dot{y}) \tag{2}$$

where $A_{\mathrm{f}}S_{\mathrm{f}}$ represents the approximated nonlinear Coulomb friction, in which the amplitude $A_{\mathrm{f}}$ may be unknown but the continuous shape function $S_{\mathrm{f}}$ is known. An example of the 10 N·m Coulomb friction approximation is presented in Fig. 2.

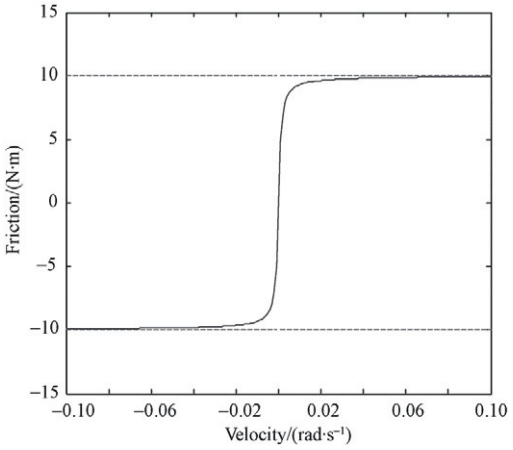


Fig. 2 Coulomb friction approximation term $A_{\mathrm{f}}S_{\mathrm{f}}$.

Thus, the dynamic Eq. (1) can be rewritten as

$$T = AP_{\mathrm{L}} - B\dot{y} - A_{\mathrm{f}} S_{\mathrm{f}}(\dot{y}) - \tilde{f}(t, y, \dot{y}) \tag{3}$$

The pressure dynamics can be written as [18]

$$\begin{cases} \dot{P}_1 = \dfrac{\beta_e}{V_1}(-A\dot{y} - C_t P_L + Q_1) \\ \dot{P}_2 = \dfrac{\beta_e}{V_2}(A\dot{y} + C_t P_L - Q_2) \end{cases} \tag{4}$$

where $\beta_e$ is the effective bulk modulus; $V_1 = V_{01} + Ay$ represents the total control volume of the first chamber, and $V_2 = V_{02} - Ay$ the total control volume of the second chamber, $V_{01}$ and $V_{02}$ are the initial volumes in the two chambers; $C_t$ is the coefficient of the internal leakage of the actuator; $Q_1$ and $Q_2$ are the supplied flow rate to the forward chamber and the return flow rate of the return chamber. $Q_1$ and $Q_2$ are related to $x_v$, by [18]

$$\begin{cases} Q_1 = k_q x_v \left[ s(x_v)\sqrt{P_s - P_1} + s(-x_v)\sqrt{P_1 - P_r} \right] \\ Q_2 = k_q x_v \left[ s(x_v)\sqrt{P_2 - P_r} + s(-x_v)\sqrt{P_s - P_2} \right] \end{cases} \tag{5}$$

where $k_q = C_d w\sqrt{2/\rho}$ ($C_d$ is the discharge coefficient, $w$ the spool valve area gradient, $\rho$ the density of oil) and $s(\bullet)$ is defined as

$$s(\bullet) = \begin{cases} 1 & \bullet \geq 0 \\ 0 & \bullet < 0 \end{cases} \tag{6}$$

The effects of servo valve dynamics have been included in some literatures [19, 22], which require an additional sensor to obtain the spool position and only minimal performance improvement is achieved for tracking performance, so many researchers neglect servo valve dynamics. Since a high-response servo valve is used here, it is assumed that the control applied to the servo valve is directly proportional to the spool position, then the following equation is given by $x_v = k_i u$, where $k_i$ is a positive constant and $u$ the input voltage. Therefore Eq. (5) can be transformed to

$$\begin{cases} Q_1 = gu\left[ s(u)\sqrt{P_s - P_1} + s(-u)\sqrt{P_1 - P_r} \right] \\ Q_2 = gu\left[ s(u)\sqrt{P_2 - P_r} + s(-u)\sqrt{P_s - P_2} \right] \end{cases} \tag{7}$$

where $g = k_q k_i$.

**Assumption 1** In practical hydraulic system under normal working conditions, $P_1$ and $P_2$ are both bounded by $P_r$ and $P_s$, i.e., $0 < P_r < P_1 < P_s$, $0 < P_r < P_2 < P_s$.

Based on Eqs. (3)-(4) and Eq. (7), the dynamic of torque control system can be described by

$$\dot{T} = \left(\frac{R_1}{V_1} + \frac{R_2}{V_2}\right) A\beta_e g u - \left(\frac{1}{V_1} + \frac{1}{V_2}\right)\beta_e A^2 \dot{y} - \left(\frac{1}{V_1} + \frac{1}{V_2}\right) A\beta_e C_t P_L - B\ddot{y} - A_f \dot{S}_f(\dot{y}) - \tilde{d}(t, y, \dot{y}) \tag{8}$$

where $\tilde{d}(t, y, \dot{y}) \triangleq \dot{\tilde{f}}(t, y, \dot{y})$; $R_1$ and $R_2$ are defined as

$$\begin{cases} R_1 = s(u)\sqrt{P_s - P_1} + s(-u)\sqrt{P_1 - P_r} > 0 \\ R_2 = s(u)\sqrt{P_2 - P_r} + s(-u)\sqrt{P_s - P_2} > 0 \end{cases} \tag{9}$$

For any torque trajectory tracking, we have the following assumption for nonlinear control.

**Assumption 2** The desired torque command $T_d(t)$ is one-order continuous and differentiable. The command $T_d(t)$ and its one-order differential are bounded. The motion disturbances $y$, $\dot{y}$ and $\ddot{y}$ are also bounded.

Given the desired torque trajectory $T_d(t)$, the objective is to synthesize a bounded control input $u$ such that the output $T$ tracks $T_d(t)$ as closely as possible in spite of various model uncertainties and uncertain nonlinearities.

## 3. Nonlinear Adaptive Robust Force Controller Design

### 3.1. Design model and issues to be addressed

In general, the system is subject to parametric uncertainties due to the variations of $B$, $A_f$, $\beta_e$, $C_t$ and $g$. In order to simplify the system equation, define the unknown but constant parameter set $\boldsymbol{\theta} = [\theta_1\ \theta_2\ \theta_3\ \theta_4\ \theta_5]^T$, where $\theta_1 = \beta_e g$, $\theta_2 = \beta_e$, $\theta_3 = \beta_e C_t$, $\theta_4 = B$, $\theta_5 = A_f$. Thus Eq. (8) can be transformed into

$$\dot{T} = \theta_1 f_1 u - \theta_2 f_2 - \theta_3 f_3 - \theta_4 \ddot{y} - \theta_5 \dot{S}_f(\dot{y}) - \tilde{d} \tag{10}$$

where the nonlinear function $f_1$, $f_2$ and $f_3$ are defined as

$$\begin{cases} f_1(P_1, P_2, y) = \left(\dfrac{R_1}{V_1} + \dfrac{R_2}{V_2}\right) A \\ f_2(y, \dot{y}) = \left(\dfrac{1}{V_1} + \dfrac{1}{V_2}\right) A^2 \dot{y} \\ f_3(P_1, P_2, y) = \left(\dfrac{1}{V_1} + \dfrac{1}{V_2}\right) A P_L \end{cases} \tag{11}$$

Since $y$ is the displacement of the actuator, considering Eq. (9) and Assumption 1, the following inequations always hold:

$$f_1(P_1, P_2, y) > 0, \quad \forall y, P_1, P_2 \tag{12}$$

Although we do not have the true values of the unknown parameter set $\boldsymbol{\theta}$, for most applications, the extent of the parametric uncertainties and uncertain nonlinearities is known. Thus the following practical assumption is made.

**Assumption 3** Parametric uncertainties and uncertain nonlinearities satisfy

$$\begin{cases} \boldsymbol{\theta} \in \Omega_{\boldsymbol{\theta}} \triangleq \{\boldsymbol{\theta} : \boldsymbol{\theta}_{\min} \leq \boldsymbol{\theta} \leq \boldsymbol{\theta}_{\max}\} \\ \left|\tilde{d}(t, y, \dot{y})\right| \leq \delta_d(t, y, \dot{y}) \end{cases} \tag{13}$$

where $\theta_{\min} = [\theta_{1\min}\ \ \theta_{2\min}\ \ \cdots\ \ \theta_{5\min}]^T$, $\theta_{\max} = [\theta_{1\max}\ \theta_{2\max} \cdots \theta_{5\max}]^T$, and $\delta_d$ is interference function.

### 3.2. Discontinuous projection mapping

Let $\hat{\boldsymbol{\theta}}$ denote the estimate of $\boldsymbol{\theta}$ and $\tilde{\boldsymbol{\theta}}$ the estimation error (i.e. $\tilde{\boldsymbol{\theta}} = \hat{\boldsymbol{\theta}} - \boldsymbol{\theta}$). Viewing Eq. (13), a discontinuous mapping can be defined as [19]

$$\mathrm{Proj}_{\hat{\boldsymbol{\theta}}}(\bullet_i)=\begin{cases}0 & \hat{\theta}_i=\theta_{i\max}\ \text{and}\ \bullet_i>0\\ 0 & \hat{\theta}_i=\theta_{i\min}\ \text{and}\ \bullet_i<0\\ \bullet_i & \text{Otherwise}\end{cases} \tag{14}$$

where $i$ =0,1, …, 5. $\bullet_i$ represents the $i$th component of the vector $\bullet$ and the operation < for two vectors is performed in terms of the corresponding elements of the vectors. Suppose that the parameter estimate $\hat{\boldsymbol{\theta}}$ is updated using the following projection type adaptation law:

$$\dot{\hat{\boldsymbol{\theta}}}=\mathrm{Proj}_{\hat{\boldsymbol{\theta}}}(\boldsymbol{\Gamma}\boldsymbol{\tau})\quad \hat{\boldsymbol{\theta}}(0)\in\Omega_{\boldsymbol{\theta}} \tag{15}$$

where $\boldsymbol{\Gamma}$ >0 is a diagonal adaptation rate matrix, and $\tau$ an adaptation function to be synthesized later. For any adaption function $\boldsymbol{\tau}$, the projection mapping used in Eq. (15) guarantees

$$\begin{aligned}&\mathbf{P1}\quad \hat{\boldsymbol{\theta}}\in\Omega_{\hat{\boldsymbol{\theta}}}\triangleq\left\{\hat{\boldsymbol{\theta}}:\boldsymbol{\theta}_{\min}\le\hat{\boldsymbol{\theta}}\le\boldsymbol{\theta}_{\max}\right\}\\ &\mathbf{P2}\quad \tilde{\boldsymbol{\theta}}^{\mathrm{T}}(\boldsymbol{\Gamma}^{-1}\mathrm{Proj}_{\hat{\boldsymbol{\theta}}}(\boldsymbol{\Gamma}\boldsymbol{\tau})-\boldsymbol{\tau})\le\mathbf{0},\quad\forall\boldsymbol{\tau}\end{aligned} \tag{16}$$

Property P1 implies that the parameter estimations are always within the known bounded set $\Omega_\theta$, that is to say, the adaptation process Eq. (15) is a controlled process. Property P2 enables one to know that the use of projection modification to the traditional discontinuous adaptation law holds the perfect learning capability of the traditional one.

Proofs of Eq. (16): the property P1 of Eq. (16) is obvious and the proof is ignored. Then we consider the proof of property P2.

Noting Eqs. (14)-(15), if in the case $\hat{\theta}_i=\theta_{i\max}$ and $\boldsymbol{\Gamma}\boldsymbol{\tau}$>0, i.e., $\mathrm{Proj}_{\hat{\boldsymbol{\theta}}}(\boldsymbol{\Gamma}\boldsymbol{\tau})=\mathbf{0}$, $\tilde{\boldsymbol{\theta}}=\hat{\boldsymbol{\theta}}-\boldsymbol{\theta}>\mathbf{0}$ and $\boldsymbol{\tau}$>$\mathbf{0}$, then $\tilde{\boldsymbol{\theta}}^{\mathrm{T}}(\boldsymbol{\Gamma}^{-1}\mathrm{Proj}_{\hat{\boldsymbol{\theta}}}(\boldsymbol{\Gamma}\boldsymbol{\tau})-\boldsymbol{\tau})=-\tilde{\boldsymbol{\theta}}^{\mathrm{T}}\boldsymbol{\tau}<\mathbf{0}$.

Noting Eqs. (14)-(15), if in the case $\hat{\theta}_i=\theta_{i\min}$ and $\boldsymbol{\Gamma}\boldsymbol{\tau}$<0, i.e., $\mathrm{Proj}_{\hat{\boldsymbol{\theta}}}(\boldsymbol{\Gamma}\boldsymbol{\tau})=\mathbf{0}$, $\tilde{\boldsymbol{\theta}}=\hat{\boldsymbol{\theta}}-\boldsymbol{\theta}<\mathbf{0}$ and $\boldsymbol{\tau}<\mathbf{0}$, then $\tilde{\boldsymbol{\theta}}^{\mathrm{T}}(\boldsymbol{\Gamma}^{-1}\mathrm{Proj}_{\hat{\boldsymbol{\theta}}}(\boldsymbol{\Gamma}\boldsymbol{\tau})-\boldsymbol{\tau})=-\tilde{\boldsymbol{\theta}}^{\mathrm{T}}\boldsymbol{\tau}<\mathbf{0}$.

In other cases, $\mathrm{Proj}_{\hat{\boldsymbol{\theta}}}(\boldsymbol{\Gamma}\boldsymbol{\tau})=\boldsymbol{\Gamma}\boldsymbol{\tau}$, then

$$\tilde{\boldsymbol{\theta}}^{\mathrm{T}}(\boldsymbol{\Gamma}^{-1}\mathrm{Proj}_{\hat{\boldsymbol{\theta}}}(\boldsymbol{\Gamma}\boldsymbol{\tau})-\boldsymbol{\tau})=\tilde{\boldsymbol{\theta}}^{\mathrm{T}}(\boldsymbol{\Gamma}^{-1}\boldsymbol{\Gamma}\boldsymbol{\tau}-\boldsymbol{\tau})=\mathbf{0}$$

This indicates that for any adaption function $\boldsymbol{\tau}$, the property P2 is always satisfied. This proofs the properties of Eq. (16).

### 3.3. Controller design

Define the following Lyapunov function $V(t)$:

$$V(t)=\frac{1}{2}e^2 \tag{17}$$

where $e$=$T$–$T_{\mathrm{d}}$ is the tracking error and its time derivative can be written as

$$\dot{e}=\theta_1 f_1 u-\theta_2 f_2-\theta_3 f_3-\theta_4\ddot{y}-\theta_5\dot{S}_{\mathrm{f}}(\dot{y})-\dot{T}_{\mathrm{d}}-\tilde{d} \tag{18}$$

Thus we can design a nonlinear adaptive robust control law $u$ such that the output tracking error $e$ converges to zero or a small value with a guaranteed transient performance. The resulting controller law is

$$\begin{cases}u=u_{\mathrm{m}}+u_{\mathrm{r}}\\ u_{\mathrm{m}}=\dfrac{1}{\hat{\theta}_1 f_1}[\hat{\theta}_2 f_2+\hat{\theta}_3 f_3+\hat{\theta}_4\ddot{y}+\hat{\theta}_5\dot{S}_{\mathrm{f}}(\dot{y})+\dot{T}_{\mathrm{d}}]\\ u_{\mathrm{r}}=\dfrac{-ke+u_{\mathrm{s}}}{f_1}\end{cases} \tag{19}$$

where $u_{\mathrm{m}}$ is the adaptive model compensation term through online parameter adaptation given by Eq. (15), $k$ a positive feedback gain, and $u_{\mathrm{s}}$ a nonlinear robust term used to dominate the model uncertainties coming from both parametric uncertainties $\tilde{\boldsymbol{\theta}}$ and uncertain nonlinearities $\tilde{d}$ with a given accuracy.

Based on this controller, the time derivative of $V$ is

$$\dot{V}=e\dot{e}=-\theta_1 k e^2+e(\theta_1 u_{\mathrm{s}}-\tilde{\boldsymbol{\theta}}^{\mathrm{T}}\boldsymbol{\varphi}-\tilde{d}) \tag{20}$$

where the regressor $\boldsymbol{\varphi}$ is defined as

$$\boldsymbol{\varphi}=[f_1 u_{\mathrm{m}}\ \ -f_2\ \ -f_3\ \ -\ddot{y}\ \ -\dot{S}_{\mathrm{f}}(\dot{y})]^{\mathrm{T}} \tag{21}$$

For the robust design, we make the robust term $u_{\mathrm{s}}$ be any function satisfying the following conditions:

$$e(\theta_1 u_{\mathrm{s}}-\tilde{\boldsymbol{\theta}}^{\mathrm{T}}\boldsymbol{\varphi}-\tilde{d})\le\varepsilon \tag{22}$$

$$eu_{\mathrm{s}}\le 0 \tag{23}$$

where $\varepsilon$ is a positive design parameter which can be arbitrarily small and represents the given robust accuracy.

Many methods can be used to choose a robust term $u_{\mathrm{s}}$ satisfying Eqs. (22)-(23). Here we give an example as follows.

Let $h$ be any smooth function satisfying

$$h\ge\|\boldsymbol{\theta}_{\mathrm{M}}\|^2\|\boldsymbol{\varphi}\|^2+\delta_{\mathrm{d}}^2 \tag{24}$$

where $\boldsymbol{\theta}_{\mathrm{M}}$= $\boldsymbol{\theta}_{\max}$–$\boldsymbol{\theta}_{\min}$. Then $u_{\mathrm{s}}$ can be chosen as

$$u_{\mathrm{s}}=-k_{\mathrm{s}}e\triangleq-\frac{h}{2\theta_{1\min}\varepsilon}e \tag{25}$$

where $k_{\mathrm{s}}$ is a positive nonlinear gain. It can be shown that Eqs. (22)-(23) are satisfied. The proofs are shown as follows.

**Proof** Eq. (23) is obviously satisfied and the proof is ignored. Then we consider the proof of Eq. (22). Substituting Eq. (25) into the left of Eq. (22) which is marked as $\Xi$, we have

$$\Xi\triangleq e(\theta_1 u_{\mathrm{s}}-\tilde{\boldsymbol{\theta}}^{\mathrm{T}}\boldsymbol{\varphi}-\tilde{d})=-\frac{h}{2\theta_{1\min}\varepsilon}\theta_1 e^2-\tilde{\boldsymbol{\theta}}^{\mathrm{T}}\boldsymbol{\varphi}e-\tilde{d}e \tag{26}$$

Noting Assumption 3, we have

$$-\frac{\theta_1 h}{2\theta_{1\min}\varepsilon}e^2-\tilde{\boldsymbol{\theta}}^{\mathrm{T}}\boldsymbol{\varphi}e-\tilde{d}e\le-\frac{h}{2\varepsilon}e^2+\|\tilde{\boldsymbol{\theta}}^{\mathrm{T}}\boldsymbol{\varphi}\|\,|e|+\delta_{\mathrm{d}}|e| \tag{27}$$

Combining the definition of $h$, we have

$$\Xi\le\underbrace{-\frac{1}{2}\frac{\|\boldsymbol{\theta}_{\mathrm{M}}\|^2\|\boldsymbol{\varphi}\|^2}{\varepsilon}e^2+\|\tilde{\boldsymbol{\theta}}^{\mathrm{T}}\boldsymbol{\varphi}\|\,|e|}_{\text{part 1}}\underbrace{-\frac{1}{2}\frac{\delta_{\mathrm{d}}^2 e^2}{\varepsilon}+\delta_{\mathrm{d}}|e|}_{\text{part 2}} \tag{28}$$

Using the Young inequation for the part 1 and part 2, we can get that

$$\Xi \le \underbrace{\frac{1}{2}\varepsilon}_{\text{part 1}} + \underbrace{\frac{1}{2}\varepsilon}_{\text{part 2}} = \varepsilon \tag{29}$$

Then Eq. (22) is satisfied.

### 3.4. Main results

**Theorem** With the projection type adaptation law Eq. (15) and adaptation function of $\boldsymbol{\tau} = \boldsymbol{\varphi} e$, the proposed adaptive robust force control law Eq. (19) guarantees that

1) In general, all signals are bounded. Furthermore, the positive definite $V$ is bounded by

$$V(t) \le \exp(-\lambda t)V(0) + \frac{\varepsilon}{\lambda}[1-\exp(-\lambda t)] \tag{30}$$

where $\lambda = 2k\theta_{1\min}$ is the exponentially converging rate.

2) If after a finite time $t_0$, $\tilde{d} = 0$, i.e., in the presence of parametric uncertainties only, in addition to results in 1), asymptotic output tracking is also achieved, i.e., $e \to 0$ as $t \to \infty$.

Proof: Noting Eq. (20) and Eq. (22), the time derivative of $V$ satisfies

$$\dot{V} \le -\theta_1 k e^2 + \varepsilon$$

Combining the definition of $\lambda$, we have

$$\dot{V} \le -\lambda V + \varepsilon$$

Therefore, using the comparison lemma [23], we can obtain the Eq. (30). Then the tracking error $e$ is bounded. From Assumption 1 and Assumption 2, $T$, $f_1$, $f_2$, $f_3$ and $\boldsymbol{\varphi}$ are bounded. From the property P1 of Eq. (16) and Assumption 3, the estimation of unknown parameter $\boldsymbol{\theta}$ is bounded. Thus $u$ is bounded. This proves the conclusion 1). Now consider the situation in 2) of Theorem. Choose a positive definite function $V_s$ as

$$V_s = V + \frac{1}{2}\tilde{\boldsymbol{\theta}}^{\mathrm{T}}\boldsymbol{\Gamma}^{-1}\tilde{\boldsymbol{\theta}}$$

Noting that the unknown parameter $\boldsymbol{\theta}$ is constant, thus we have

$$\dot{\tilde{\boldsymbol{\theta}}} = \dot{\hat{\boldsymbol{\theta}}} - \dot{\boldsymbol{\theta}} = \dot{\hat{\boldsymbol{\theta}}}$$

Then the time derivative of $V_s$ is

$$\dot{V}_s = \dot{V} + \tilde{\boldsymbol{\theta}}^{\mathrm{T}}\boldsymbol{\Gamma}^{-1}\dot{\hat{\boldsymbol{\theta}}}$$

From Eq. (20) and Eq. (23), we obtain

$$\dot{V}_s = -\theta_1 k e^2 + e(\theta_1 u_s - \tilde{\boldsymbol{\theta}}^{\mathrm{T}}\varphi) + \tilde{\boldsymbol{\theta}}^{\mathrm{T}}\boldsymbol{\Gamma}^{-1}\dot{\hat{\boldsymbol{\theta}}} \le$$

$$-\theta_1 k e^2 + \tilde{\boldsymbol{\theta}}^{\mathrm{T}}(\boldsymbol{\Gamma}^{-1}\dot{\hat{\boldsymbol{\theta}}} - \boldsymbol{\varphi} e)$$

Noting the definition of $\boldsymbol{\tau}$ and the property P2 of Eq. (16), then

$$\dot{V}_s \le -\theta_1 k e^2 \triangleq -W$$

That is to say, $V_s \le V_s(0)$. Therefore, $W \in L_2$ and $V_s \in L_\infty$. Since all signals are bounded, from Eq. (18), it is easy to check that $\dot{W}$ is bounded and thus uniformly continuous. By Barbalat's lemma, $W \to 0$ as $t \to \infty$, which leads to 2) of Theorem.

From Eq. (31) and noting the definition of $V$ in Eq. (17), the tracking error can always be bounded by

$$|e| \le \sqrt{2\exp(-\lambda t)V(0) + \frac{2\varepsilon}{\lambda}[1-\exp(-\lambda t)]} \tag{31}$$

That is to say, results in 1) of Theorem indicate that the proposed controller has an exponentially convergence transient performance with the exponentially converging rate $\lambda$ and the final tracking error being able to be freely adjusted via certain controller parameters in a known form; it is seen from Eq. (31) that $\lambda$ can be made arbitrarily large, and $\varepsilon/\lambda$, the bound of $e(\infty)$ (an index for the final tracking errors), can be made arbitrarily small by increasing gains $k$ and/or decreasing controller parameter $\varepsilon$. Such a guaranteed transient performance is especially important for the control of electro-hydraulic systems since execute time of a run is very short. 2) of Theorem implies that the parametric uncertainties may be reduced through parameter adaptation and an improved performance is obtained.

Knowing the robust law Eq. (25), we may implement the needed robust control term in the following two ways. The first method is to pick up a set of values $\boldsymbol{\theta}_M$, $\|\boldsymbol{\varphi}\|$, $\delta_d$, and $\varepsilon$ to calculate the right-hand side of Eq. (25). So that Eq. (25) is satisfied for a guaranteed global stability and a guaranteed control accuracy. This approach is rigorous and should be the formal approach to choose. However, it increases the complexity of the resulting control law considerably since it may need significant amount of computation time to calculate the lower bound of $h$. As an alternative, a pragmatic approach is to simply choose $k_s$ large enough without worrying about the specific values of $\boldsymbol{\theta}_M$, $\|\boldsymbol{\varphi}\|$, $\delta_d$ and $\varepsilon$. By doing so, Eq. (25) will be satisfied for certain sets of these values, at least locally around the desired trajectory to be tracked. In this paper, the second approach is used since it not only reduces the online computation time significantly, but also facilitates the gain tuning process in implementation.

## 4. Simulation and Experimental Results

### 4.1. Simulation results

To illustrate the above designs, simulation results are obtained for EHLS discussed in Section 2, with the following actual parameters: $A = 2\times10^{-4}$ m$^3$/rad, $B$=80 N·m·s/rad, $\beta_e = 2\times10^8$ Pa, $C_t = 9\times10^{-12}$ m$^5$/(N·s), $g = 4\times10^{-8}$ m$^4$/(s·V·$\sqrt{\text{N}}$), $P_s = 21\times10^6$ Pa, $P_r = 0$ Pa, $V_{01} = V_{02} = 1.7\times10^{-4}$ m$^3$, $A_f$=80 N·m, $S_f$=2arctan(10 $\dot{y}$ )/π. Hence the actual value of $\boldsymbol{\theta}$ is $\boldsymbol{\theta}$= [8 $2\times10^8$ $1.8\times10^{-3}$ 80 800]$^{\mathrm{T}}$, and the uncertain nonlinearity term $\tilde{d}$ =0. The aircraft actuator system has the same actual pa-

rameters but with an inertial load $J$=0.32 kg·m$^2$ to simulate the motion disturbance.

The controller parameters are as follows: feedback gain $K=k+k_s=100$, and the bounds of uncertain ranges are given by $\boldsymbol{\theta}_{max}=[10\ 3\times10^{8}\ 3\times10^{-3}\ 100\ 100]^T$, $\boldsymbol{\theta}_{min}=[6\ 10^{8}\ 10^{-3}\ 60\ 60]^T$. The initial estimate of $\boldsymbol{\theta}$ is chosen as $\boldsymbol{\theta}(0)=\boldsymbol{\theta}_{min}$, which satisfies Eq. (13) but differs significantly from its actual value $\boldsymbol{\theta}$ to test the effect of parametric uncertainties. The adaptation gain $\boldsymbol{\Gamma}=\text{diag}\{6\times10^{-4},\ 10^{11},\ 3\times10^{-11},\ 20,\ 200\}$. A sampling period of 0.5 ms is used in all simulation.

To test the nominal tracking performance of the proposed controller, simulations are first run for the case that the motion disturbance has the same frequency with torque trajectory. The desired torque trajectory is $T_d=1\ 000\sin(3.14t)[1-\exp(-0.5t^3)]$ N·m and the motion disturbance is given by $y=0.2\cdot\sin(3.14t)\cdot[1-\exp(-0.5t^3)]$ rad which satisfy Assumption 2. The torque tracking performance is shown in Fig. 3 and the control input in Fig. 4. As shown, the proposed controller has very small tracking errors and after the starting periods, the tracking error is converging to zero, which verifies the excellent tracking capability of the proposed adaptive algorithms. The parameter estimation is shown in Fig. 5.

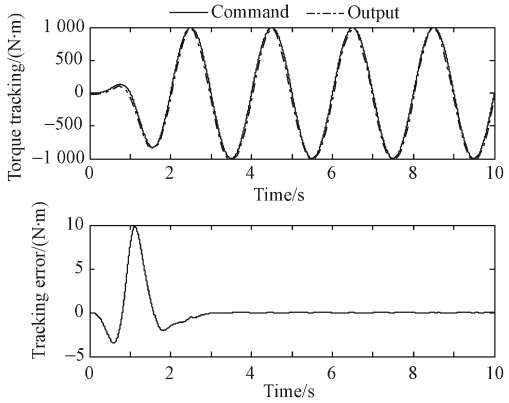


Fig. 3 Torque tracking performance with the same frequency disturbance.

Although the convergence of parameter estimation is not very good because the estimation law in Eq. (15) is direct-type adaptation law, which normally does not lead to accurate estimate of parameters, the adaptive model compensation proposed in this paper also makes the tracking error go to a very small value, so the parameter estimation is not shown in the next experimental comparison. In addition, from the estimation of $\theta_5$, in the starting periods, the adaptive estimation is controlled to a given extent, which is the purpose of adding the projection Eq. (14) into the adaptation process Eq. (15). The total control effort $u$ is mainly coming from the adaptive model compensation $u_m$ in Fig. 4. Although the motion disturbance exists in EHLS, the proposed controller captures the exact structure information and adapts these structure amplitudes, and that is the reason why the tracking error becomes small under motion disturbance.

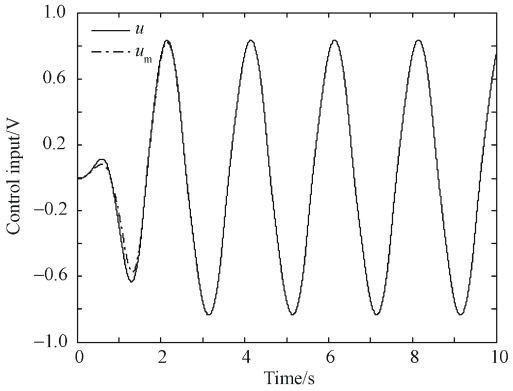


Fig. 4 Control input with the same frequency disturbance.

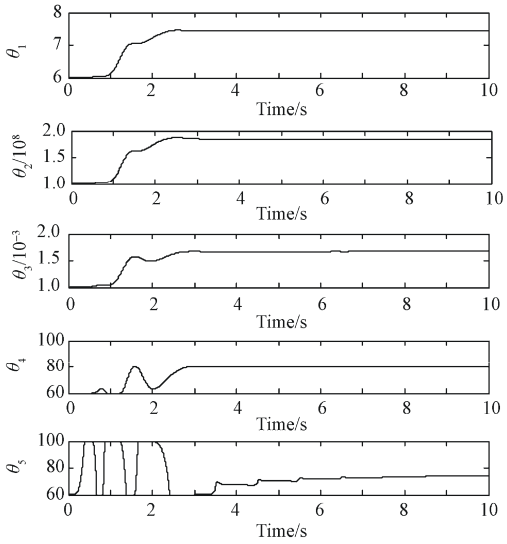


Fig. 5 Parameter estimation with the same frequency disturbance.

To test the tracking performance at different frequencies of motion disturbance, the motion trajectory is changed to $y=0.349\sin(6.28t)[1-\exp(-0.5t^3)]$ rad. Under this condition, the EHLS tracking performance is shown in Fig. 6 and control input in Fig. 7. Although the motion disturbance has greatly increased, the tracking error is a little larger, and after the starting period, the tracking error converges to a low level,

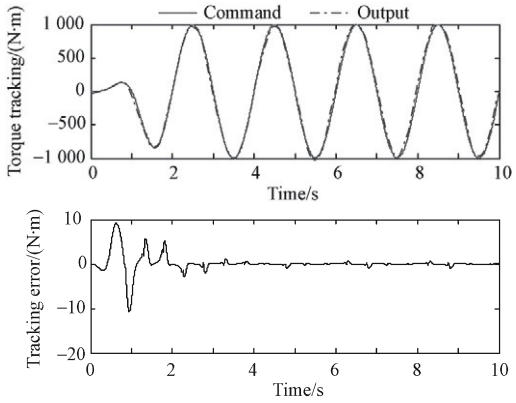


Fig. 6 Torque tracking performance with different frequency disturbances.

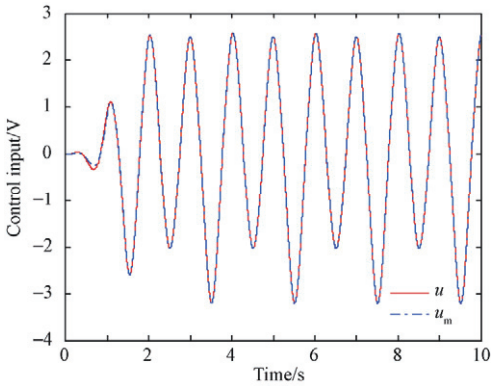


Fig. 7 Control input with different frequency disturbances.

which verifies the proposed nonlinear adaptive robust force controller.

### 4.2. Comparative experimental results

The experimental platform is shown in Fig. 8. This platform consists of bench case, EHLS and a motion actuator. All actuators have the same parameter given in simulation. In Fig. 8, the left part acts as the EHLS and the right one acts as the aircraft actuator system which is used to produce the motion disturbance. The specifications of the test apparatus shown in Fig. 8 are listed in Table 1. The sampling time is 0.5 ms. The hydraulic servo valve is Moog G761-3005 whose bandwidth is about 100 Hz.

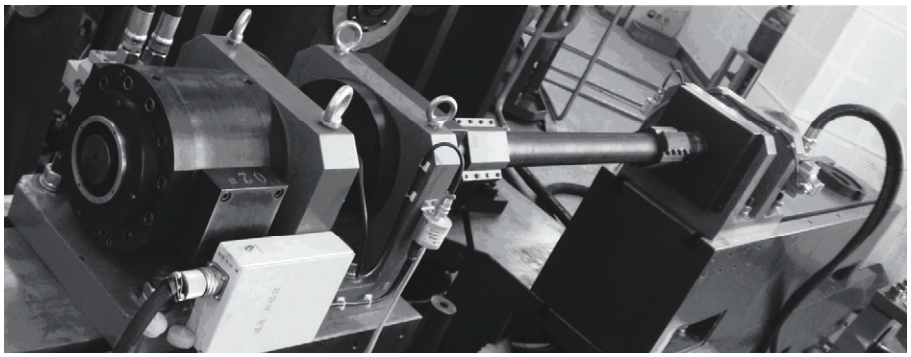

Fig. 8 Experimental test rig.

**Table 1 Specifications of the EHLS and aircraft actuation system**

| Component | Specification | Value | Component | Specification | Value |
|---|---|---|---|---|---|
| Hydraulic supply | Number | 2 | Torque sensor | Number | 2 |
| | System pressure/bar | 210 | | Range/(N·m) | −2 800-2 800 |
| | Max continuous flow rate/ ($L\cdot min^{-1}$) | 120 | | Accuracy/% | 0.3 |
| Servo valve | Number | 2 | Angular sensor | Number | 2 |
| | Type | Moog G761-3005 | | Type | Renishaw RGH20 |
| | Rated flow/($L\cdot min^{-1}$) | 63 | | Accuracy/% | 20 |
| Hydraulic actuator | Number | 2 | A/D card | Type | Advantech PCI-1716 |
| | Rotary range/(°) | −35-35 | D/A card | Type | Advantech PCI-1723 |
| | Radian displacement/ ($L\cdot rad^{-1}$) | 0.191 67 | Counter | Type | NI PCI-6601 |
| | Stall torque/(N·m) | 2 300 | Computer | Type | IEI WS-855GS |

The conventional PID controller widely used in industry and the proposed adaptive robust controller (ARC) in this paper are compared. The optimized PID controller parameters are $k_p$=0.063, $k_i$=1, $k_d$=1×10$^{-6}$, which are tuned through try-and-error. One may argue that larger PID parameters can make better tracking performance. But these parameters are achieved ultimately and larger parameters will lead the system to be unstable. Thus using the PID controller with these parameters to compare with the proposed ARC controller is fair. The experimental test is first run at the same frequency. The aircraft actuator system plays sinusoidal movement of 10° amplitude and the frequency is 2 Hz. The torque command is 2 000 N·m at the same frequency. The results of the torque tracking performance and control output with PID controller are shown in Fig. 9 and those of the proposed ARC controller in Fig. 10. The corresponding response results of the motion actuator are shown in Figs. 11-12 respectively. It is clear from the comparative results of the torque tracking performance that the proposed ARC controller achieves excellent tracking errors than PID controller from the maximum tracking error 200 N·m to 50 N·m. In addition, the motion disturbance is severe in this experiment which can be indicated by the control input of the aircraft actuator system whose maximum amplitude (7.5 V) almost approaches the maximum control authority (10 V). The severe disturbance may lead to a much degraded performance with conventional closed-loop controllers (like PID controller).

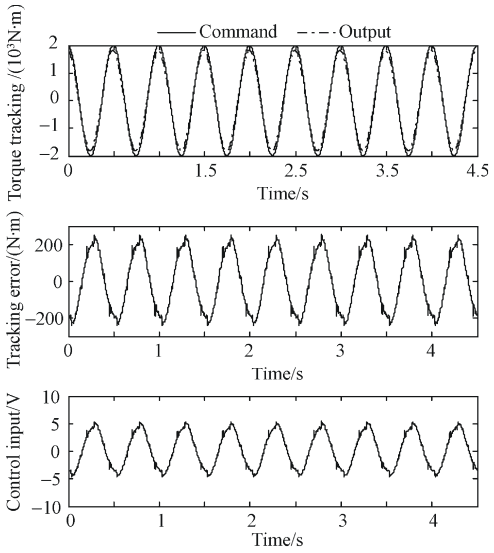


Fig. 9 Torque tracking performance under PID controller.

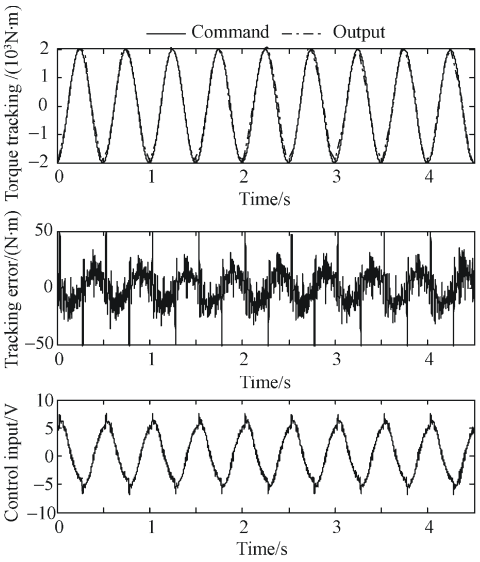


Fig. 10 Torque tracking performance under ARC controller.

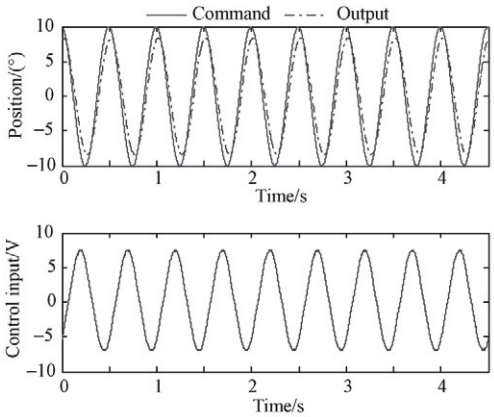


Fig. 11 Response results of aircraft actuator under PID controller.

The experimental test is then run in a different frequency case. The aircraft actuator system plays sinusoidal movement of 20° amplitude and the frequency is 1 Hz. The torque command is the sinusoidal signal with 1 000 N·m amplitude and 5 Hz frequency. The torque tracking performance under PID controller is shown in Fig. 13 and the proposed controller in Fig. 14. The corresponding response results of the motion

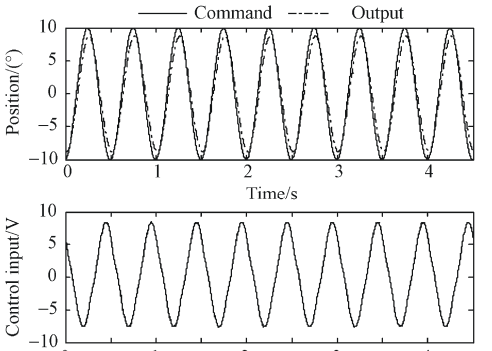


Fig. 12 Response results of aircraft actuator under ARC controller.

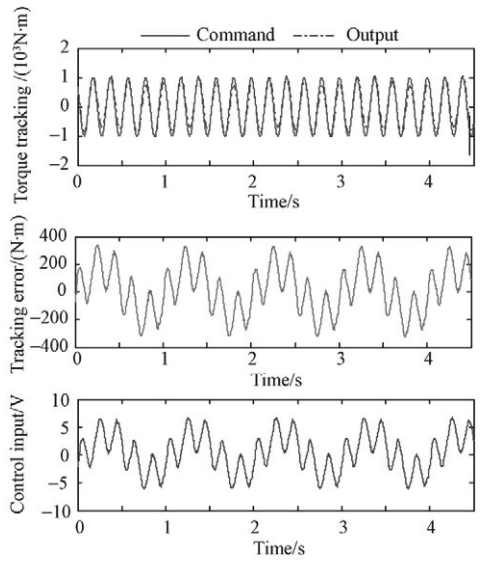


Fig. 13 Torque tracking performance under PID controller with different frequency disturbances.

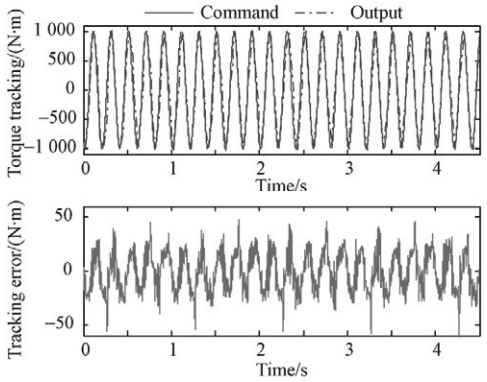


Fig. 14 Torque tracking performance under ARC controller with different frequency disturbances.

actuator are shown in Figs. 15-16 respectively. As a result, the maximum tracking error which is approximately 50 N·m is achieved by ARC controller, while the maximum tracking error is huge under the conventional PID controller. The ARC total control input $u$ mainly comes from the adaptive model compensation $u_m$ in Fig. 17.

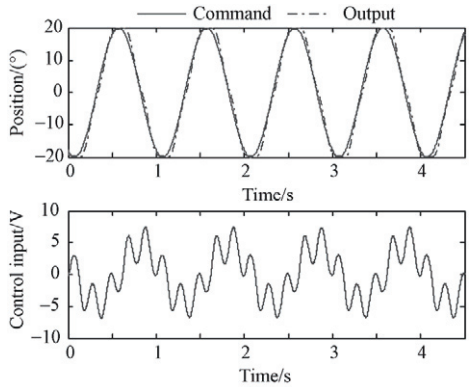


Fig. 15 Response results of aircraft actuator under PID controller with different frequencies disturbance.

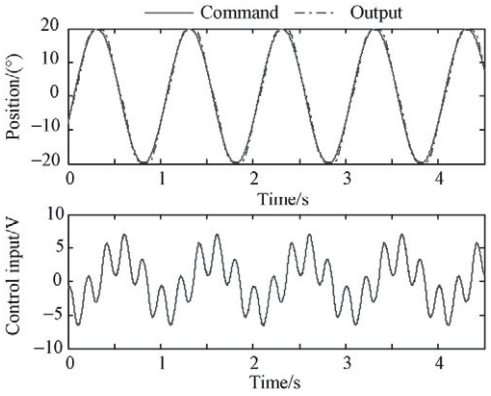


Fig. 16 Response results of the aircraft actuator under ARC controller with different frequencies disturbances.

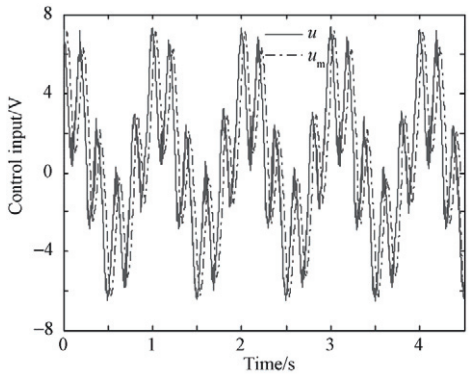


Fig. 17 ARC control input with different frequency disturbance experiments.

These results reveal clearly what the ARC controller does, i.e., the model compensation term $u_m$ acts the mainly control effort by using the nonlinear feedback to linearize the system nonlinear model. Meanwhile, the parameter uncertainties of the system are handled by the on-line learning adaptive law, thus the rest we have to do is stabilize the uncompensated terms, like unmodeled frictions and estimation errors, by a robust feedback law $u_s$.

## 5. Conclusions

In this paper, instead of many previous linear controls for hydraulic load simulator, a nonlinear adaptive robust force control has been proposed based on a nonlinear system model in which almost all important parameters are considered unknown and a nonlinear approximation of Coulomb friction is made. The proposed controller takes into account the particular nonlinearities with EHLS and derives a stable parameter adaptation to eliminate the effect of unknown but constant parametric uncertainties. Uncertain nonlinearities such as unmodeled friction forces, external disturbance and ignored high-frequency dynamics are effectively handled via certain robust feedback for a guaranteed robust performance. The controller achieves a guaranteed transient performance and final tracking accuracy for the output tracking. The performance theorem indicates that in the presence of parametric uncertainties only, asymptotic output tracking can also be achieved by the proposed controller. Extensive simulation and experiment results are obtained for an EHLS test rig to verify the high-performance nature of the proposed controller. Although the experimental results have larger tracking errors than the simulation results do because uncertain nonlinearities are not considered in simulation, the proposed adaptive robust force controller also achieves an excellent tracking performance than conventional PID controller.

## References

[1] Yu C Y, Liu Q H, Zhao K D. Velocity feedback in load simulator with a motor synchronizing in position. Journal of Harbin Institute of Technology (New Series) 1998; 5(3): 78-81.

[2] Jiao Z X, Gao J X, Hua Q, et al. The velocity synchronizing control on the electro-hydraulic load simulator. Chinese Journal of Aeronautics 2004; 17(1): 39-46.

[3] Wang X, Sun L, Yan J. Experimental research on improving loading performance by compounding feed-forward control. Journal of System Simulations 2004; 16(7): 1539-1541. [in Chinese]

[4] Yao J Y, Shang Y X, Jiao Z X. The velocity feed-forward and compensation on eliminating extraneous torque of electro-hydraulic load simulator. Proceedings of the Seventh International Conference on Fluid Power Transmission and Control, 2009; 462-465.

[5] Yao J Y, Jiao Z X, Shang Y X, et al. Adaptive nonlinear optimal compensation control for electro-hydraulic load simulator. Chinese Journal of Aeronautics 2010; 23(6): 720-733.

[6] Yao J Y, Jiao Z X. Friction compensation for hydraulic load simulator based on improved LuGre friction mode. Journal of Beijing University of Aeronautics and Astronautics 2010; 37(7): 812-815. [in Chinese]

[7] Truong D Q, Ahn K K. Force control for hydraulic load

simulator using self-turning grey predictor-fuzzy PID. Mechatronics 2009; 19(2): 233-246.
[8] Ahn K K, Truong D Q, Thanh T Q, et al. Online self-tuning fuzzy proportional-integral-derivative control for hydraulic load simulator. Journal of Systems and Control Engineering 2008; 222(2): 81-95.
[9] Nam Y, Sung K H. Force control system design for aerodynamic load simulator. Control Engineering Practice 2002; 10(5): 549-558.
[10] Nam Y. QFT force loop design for the aerodynamic load simulator. IEEE Transaction on Aerospace and Electronic Systems 2001; 37(4): 1384-1392.
[11] Truong D Q, Ahn K K. Self-tuning quantitative feedback theory for parallel force/position control of electro-hydrostatic actuators. Journal of Systems and Control Engineering 2009; 223(14): 537-556.
[12] Ahn K K, Truong D Q. Self-tuning quantitative feedback theory for force control of an electro-hydraulic test machine. Control Engineering Practice 2009; 17(11): 1291-1306.
[13] Ahn K K, Thai N H, Truong D Q. Robust force control of a hybrid actuator using quantitative feedback theory. Journal of Mechanical Science and Technology 2007; 21(12): 2048-2058.
[14] Plummer A R. Robust electro-hydraulic force control. Journal of Systems and Control Engineering 2007; 221(2): 717-731.
[15] Wang X M, Liu W G. Neural network internal feedback control for electro-hydraulic servo loading. Acta Aeronautica et Astronautica Sinica 2007; 28(3): 690-694. [in Chinese]
[16] Zhang B, Zhao K D, Sun F Y. Neural network parameter identification of electro-hydraulic load simulator. Acta Aeronautica et Astronautica Sinica 2009; 30(2): 374-379. [in Chinese]
[17] Mare F C. Dynamic loading systems for ground testing of high speed aerospace actuators. Aircraft Engineering and Aerospace Technology: An International Journal 2006; 78(4): 275-282.
[18] Merritt H E. Hydraulic control systems. New York: Wiley, 1967.
[19] Yao B, Bu F P, Reedy J, et al. Adaptive robust motion control of single-rod hydraulic actuators: theory and experiments. IEEE/ASME Transactions on Mechatronics 2000; 5(1): 79-91.
[20] Yao J Y, Jiao Z X, Huang C. Compound control for electro-hydraulic positioning system based on dynamic inverse model. Journal of Mechanical Engineering 2011; 47(10): 145-151. [in Chinese]
[21] Yao B, Al-Majed M, Tomizuka M. High performance robust motion control of machine tools: an adaptive robust control approach and comparative experiments. IEEE/ASME Transactions on Mechatronics 1997; 2(2): 63-76.
[22] Alleyne A, Liu R. A simplified approach to force control for electro-hydraulic systems. Control Engineering Practice 2000; 8(12): 1347-1356.
[23] Khalil H K. Nonlinear systems. 3rd ed. New York: Prentice Hall, 2002; 102-103.

## Biographies:

**YAO Jianyong** received B.S. degree from Tianjin University in 2006 and now is a Ph.D. candidate in School of Automation Science and Electric Engineering, Beihang University. He has published about 10 research papers in mechanical servo control systems. His main research interests lie in hydraulic servo control, adaptive control, robust control, mechatronics and hardware in the loop simulation.
E-mail: jerryyao.buaa@gmail.com

**JIAO Zongxia** is a professor of Ph.D. degree and president of School of Automation Science and Electric Engineering, Beihang University. His main research interests are fluid power transmission and control, mechatronics systems, and simulation engineering.
E-mail: zxjiao@buaa.edu.cn

**YAO Bin** received the B.E. degree in applied mechanics from Beihang University in 1987, the M.E. degree in electrical engineering from the Nanyang Technological University in 1992, and the Ph.D. degree in mechanical engineering from the University of California in 1996. Since 1996, he has been with the School of Mechanical Engineering, Purdue University, West Lafayette, IN, where he was promoted to the rank of associate professor in 2002 and professor in 2007. He was honored as a Kuang-piu Professor in 2005 and a Chang Jiang Chair Professor in 2010 at Zhejiang University, as well. His research interests include the design and control of intelligent high performance coordinated control of electro-mechanical/hydraulic systems, optimal adaptive and robust control, nonlinear observer design and neural networks for virtual sensing, modeling, fault detection, diagnostics, and adaptive fault-tolerant control, and data fusion. He has published significantly on the subjects with well over 150 technical papers while enjoying the application of the theory through industrial consulting.
E-mail: byao@purdue.edu

**SHANG Yaoxing** is an assistant professor of Ph.D. degree in School of Automation Science and Electric Engineering, Beihang University. His main research interests are mechanical design and hardware in the loop simulation.
E-mail: syxstar@gmail.com